Dependence of the structure and dynamics of liquid silicon on the choice of density functional approximation

Richard C. Remsing* and Michael L. Klein†
Institute for Computational Molecular Science and Department of Chemistry, Temple University, Philadelphia, Pennsylvania 19122, USA

Jianwei Sun‡
Department of Physics, University of Texas at El Paso, El Paso, Texas 79968, USA
(Received 13 March 2017; revised manuscript received 5 June 2017; published 19 July 2017)

In addition to its technological relevance, silicon poses a challenge for first principles simulations because it undergoes a semiconductor-to-metal transition upon melting. Moreover, the resulting metallic liquid contains a mixture of metallic and covalent bonding. This coexistence of fundamentally different interactions is difficult to describe within approximate density functional methods, which oftentimes cannot accurately describe these two extremes simultaneously. We report an investigation of the structure, dynamics, and thermodynamics of liquid silicon using *ab initio* molecular dynamics simulations with three density functional approximations: the local density approximation, the Perdew-Burke-Ernzerhof generalized gradient approximation, and the strongly constrained and appropriately normed (SCAN) meta-generalized gradient approximation. We demonstrate that SCAN describes this liquid with better accuracy than the other often-used functionals because it can simultaneously capture covalent and metallic bonding with similar high accuracy.

DOI: 10.1103/PhysRevB.96.024203

I. INTRODUCTION

Silicon is a material of great significance, forming the basis for many technological industries, including semiconductors and solar cells. Understanding its physical properties across the phase diagram is of paramount importance to more efficiently control the synthesis of Si-based materials. However, silicon, like many other tetravalently bonded semiconductors, has a quite rich phase diagram. In particular, silicon undergoes a semiconductor-metal transition upon melting, resulting in a complex metallic liquid with some fraction of transient covalent character remaining. This competition between metallic and covalent bonding can lead to a variety of interesting properties or anomalies [1–17].

Describing the delicate balance of covalent and metallic bonding in liquid silicon (l-Si) and other materials has proved to be quite a challenge. Indeed, DFT-based simulations of l-Si have not been able to quantitatively and sometimes even qualitatively predict essential structural and dynamic features [1–13]. In order to predict materials properties with confidence, especially those that contain multiple types of interactions, we need to assess the utility and limitations of the various DF approximations. In this work, we compare the descriptions of l-Si provided by three DF approximations, the local density approximation (LDA), the Perdew-Burke-Ernzerhof (PBE) generalized gradient approximation (GGA), and the strongly constrained and appropriately normed (SCAN) meta-GGA.

The LDA is the simplest and earliest DF approximation that depends on the electron density, and is derived exactly from a uniform electron gas. This approximation is often used to describe simple metals with good accuracy. However, LDA often fails for covalent bonding, like that transiently observed in l-Si. The PBE functional, and GGAs in general, improve upon the LDA by including knowledge of both the density and its gradient, giving it semilocal character [18]. This additional information enables PBE to accurately describe covalent bonding in molecules and solids, and is a significant improvement over LDA. Yet, it still lacks the quantitative accuracy desired in a first principles approach, and PBE does not describe all interactions on an equal footing [19,20].

The SCAN DF approximation provides an accurate description of virtually all types of atomic interactions, including metallic and covalent bonding [19–22]. SCAN, and meta-GGAs in general, move beyond GGAs by additionally requiring knowledge of the kinetic energy density. SCAN takes advantage of the flexibility arising from the inclusion of the kinetic energy density to satisfy the 17 known exact constraints appropriate to semilocal functionals. Moreover, SCAN is nonempirical in nature. Its parameters are not fit to any experimental data set, but are obtained by reproducing properties of several appropriate norms, like the uniform electron gas and the hydrogen atom, for which semilocal functionals can be exact or near exact [21]. However, like all local and semilocal density functionals, SCAN lacks long-ranged van der Waals (vdW) interactions, although it does capture intermediate-range many-body vdW interactions. Corrections have additionally been developed to enable a description of vdW interactions on longer length scales [23,24]. In this work, we demonstrate that SCAN provides an improved description of l-Si with respect to LDA and PBE due to better discrimination between metallic and covalent bonding.

*rremsing@temple.edu
†mlklein@temple.edu
‡jsun@tulane.edu;
Present address: Department of Physics and Engineering Physics, Tulane University, New Orleans, LA 70118, USA.

II. SIMULATION DETAILS

Born-Oppenheimer molecular dynamics (BOMD) simulations were performed using the Vienna *ab initio* simulation

package (VASP) [25]. Electron orbitals were represented by plane waves with an energy cutoff of 300 eV and considered only the Γ point for Brillouin zone sampling; a study of convergence with respect to the energy cutoff is detailed in Appendix B. The electronic structure calculations were performed within the framework of the projector augmented wave method [26]. DFT calculations were performed using the LDA, the PBE GGA [18], and the SCAN meta-GGA [21]. Spin polarization was not included in these calculations. Additional (shorter) simulations including spin polarization for both LDA and SCAN were also performed and a brief comparison between spin-polarized and non-spin-polarized results is presented in Appendix C.

Simulation cells consisted of 216 Si atoms, initially placed in the diamond lattice configuration (a $3 \times 3 \times 3$ supercell). A systematic study of finite size effects with respect to the number of atoms in the system is described in Appendix A and suggests that a 216 atom cell is sufficiently converged. The system was heated to 2500 K by velocity rescaling to obtain a liquid; melting was monitored through the appropriate Steinhardt-Nelson-Ronchetti order parameter [27], Q_6, which drops from nearly 0.6 in the solid phase to roughly 0.04 in the liquid over roughly 0.3 ps, indicating a transition to the liquid phase on this time scale. The system was further simulated at 2500 K for a total of 1.25 ps to ensure equilibration, before cooling to $T = 1800$ K. Equilibration runs of at least 10 ps and production runs of at least 29 ps were performed in the isothermal-isobaric (constant NPT) ensemble with a time step of 3 fs using a Parrinello-Rahman barostat [28] and Langevin thermostat [29,30] to maintain the pressure and temperature at $P = 0$ Pa and $T = 1800$ K, respectively.

III. RESULTS AND DISCUSSION

A. Liquid structure

We begin by discussing the structure in the various models of l-Si, because these structural differences underlie many of the differences observed in dynamic and thermodynamic properties among the three descriptions. Figure 1 compares the pair correlation functions, $g(r)$, and structure factors, $S(k)$, from the theoretical calculations and experimental x-ray diffraction measurements [31]. The position of the first peak of the SCAN $g(r)$ is in excellent agreement with that of experiment, while those of LDA and PBE are shifted to slightly larger distances. The peak height is too low in all simulated systems, indicating that these systems are slightly undercoordinated with respect to the experimental results.

The SCAN description of l-Si leads to a pronounced second peak in $g(r)$, as in the experimental results, albeit shifted to larger distances. Such a pronounced second peak is lacking in both LDA and PBE descriptions. This peak has been attributed to correlations arising from covalent bonding. Its prominence in the SCAN $g(r)$ suggests that l-Si as described by this functional has an increased amount of transient covalent bond formation with respect to LDA and PBE. This second peak is at larger distances than that determined by experiment; we will return to this point after discussing three-body correlations. The third peak in $g(r)$ is out of phase with that of experiment for all simulated systems.

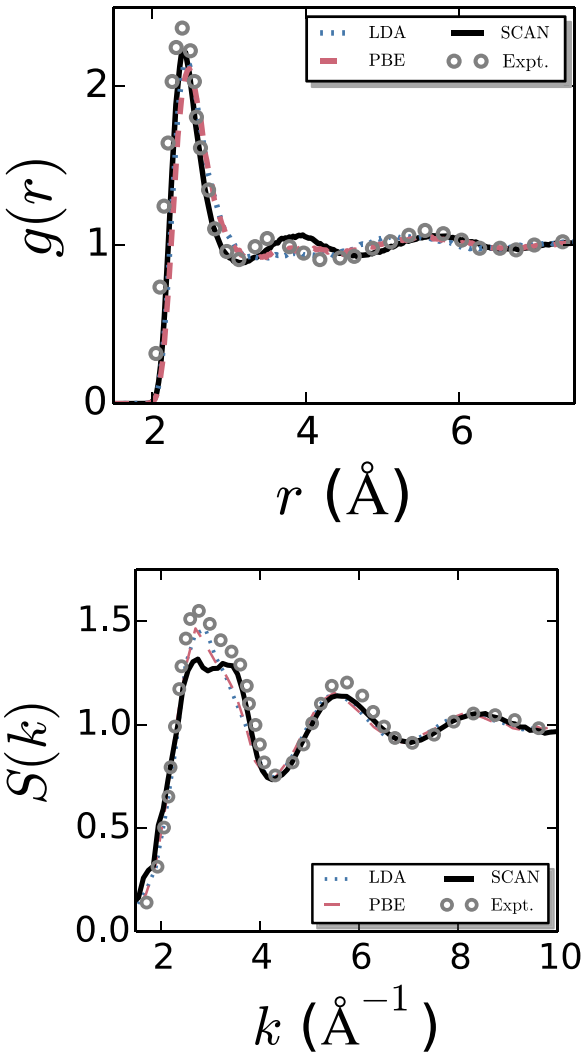

FIG. 1. (Top) Pair correlation function, $g(r)$, and (bottom) structure factor, $S(k)$, between Si atoms using SCAN, LDA, and PBE. Also shown are experimental results (Expt.) obtained by x-ray diffraction at 1793 K [31].

Figure 1 also depicts the structure factors, $S(k)$, for the various systems, where

$$S(k) = \frac{1}{N}\left\langle \sum_{i=1}^{N}\sum_{j=1}^{N} e^{-i\mathbf{k}\cdot(\mathbf{r}_i - \mathbf{r}_j)} \right\rangle \tag{1}$$

was computed directly and not from the Fourier transform of the pair correlation function. l-Si displays a shoulder in the first peak of $S(k)$ around 3.35 Å^{-1}, and all three representations of the liquid have this feature to some extent. This shoulder can be attributed to covalent tetrahedral structures in the liquid [10,32]. Therefore, the overemphasis of this shoulder at $k \approx 3.35$ Å^{-1} relative to the peak at slightly lower k indicates that SCAN may be overly covalent, most likely due to self-interaction errors. In contrast, both LDA and PBE overemphasize the lower k peak relative to the shoulder at $k \approx 3.35$ Å^{-1}. This suggests that the LDA and PBE descriptions of l-Si are less covalent than SCAN and the experimental results, such that these functionals overly favor metallic bonding

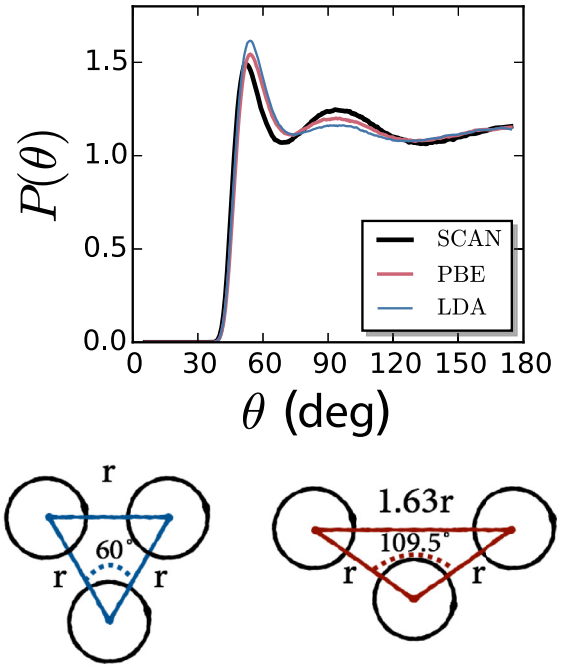

FIG. 2. (Top) Probability distributions of the angle θ formed by a central atom and two of its nearest neighbors from SCAN, LDA, and PBE. The cutoff defining the nearest-neighbor shell is the distance of the first minimum in $g(r)$. Note that the variations in the solid angle ($\sin\theta$) have been removed. (Bottom) Sketch of three particle correlations, illustrating the close-packed structure obtained when (left) $\theta = 60^\circ$ and the open structure obtained when (right) $\theta = 109.5^\circ$.

with respect to covalent bonds. We also note that all three functionals predict the same length scales for the main peak and the shoulder, in agreement with experiment. However, the subsequent peaks in LDA and PBE are slightly out of phase with respect to those determined by x-ray scattering, while SCAN produces second and third peak positions in agreement with the experimental results.

Triplet correlations are also important in l-Si. The system has directional forces due to the transient covalent character in the liquid. Thus we also compute the probability distribution of the Si-Si-Si bond angle, θ, for atoms within the first coordination shell, defined by the location of the first minimum in $g(r)$. Distributions obtained for the PBE, LDA, and SCAN descriptions of l-Si, shown in Fig. 2, display the same qualitative features, namely, a peak near $\theta = 60^\circ$ arising from noncovalent neighbors and another near the tetrahedral angle, $\theta \approx 109.5^\circ$, attributed to neighbors that are covalently bonded. These three-particle angles are sketched in the bottom of Fig. 2. The latter peak is enhanced in SCAN, relative to PBE and LDA, suggesting that the SCAN description of l-Si has more tetrahedral covalent character. Correspondingly, the noncovalent neighbor peak at low angles is reduced in SCAN relative to LDA and PBE. The PBE distribution falls between SCAN and LDA for nearly all θ, suggesting that the PBE description of l-Si has more covalent bonding than LDA, but less than SCAN.

Knowledge of the three-body angular correlations in l-Si and its relation to covalent bonding enables us to determine the origin of the second peak in $g(r)$. The first peak in $g(r)$ is located at $r \approx 2.4$ Å, and corresponds to r in the angle sketches in the bottom of Fig. 2. For noncovalently bonded atoms in the first coordination shell, nearest-neighbor distances are also r, as shown as the top leg of the triangle for $\theta = 60^\circ$. In contrast, when two atoms in the first coordination shell are covalently bonded to a central atom, the Si-Si-Si angle is $\theta \approx 109.5^\circ$, and the distance between these two atoms is $1.63r \approx 3.9$ Å, in good agreement with the computed $g(r)$ for SCAN. Thus we can conclude that the second peak in $g(r)$ is indeed due to correlations between covalently bonded neighbors. Moreover, the experimental second peak is at small distances, corresponding to a less tetrahedral and covalent liquid than predicted by SCAN.

We conclude the analysis of the structure of l-Si with a discussion of fluctuations in the coordination structure around a central Si atom. The coordination number N_C is defined as the number of atoms within the first coordination shell of a central atom,

$$N_C = 4\pi\rho \int_0^{r_{\min}} dr\, r^2 g(r), \tag{2}$$

where ρ is the bulk density and $r_{\min}$ is the position of the first minimum in $g(r)$. The first minimum is ill defined for PBE and LDA, so we use $r_{\min}$ determined from the SCAN simulations for all systems.

Probability distributions of the coordination number, $P(N_C)$, are shown in Fig. 3 and were computed by monitoring N_C for each atom in every sampled configuration of the liquid. SCAN and PBE lead to nearly the same mean, $\langle N_C\rangle_{\rm SCAN} = 6.2$ and $\langle N_C\rangle_{\rm PBE} = 6.4$, respectively. In contrast, LDA leads to a significantly higher coordination number with $\langle N_C\rangle_{\rm LDA} = 6.9$. The higher coordination number in the LDA description is a result of the higher density of that system (discussed in the next section) arising from the prevalence of metallic bonding in this description; employing Eq. (2) with the LDA $g(r)$ but the SCAN or PBE ρ leads to an $\langle N_C\rangle$ in agreement with those functionals. We also note that the $\langle N_C\rangle$ can be corrected even using LDA by artificially fixing the density of the system at the experimental one or altering the pressure (empirically) to obtain the experimental density [1,17], because this functional cannot predict the experimental density (or pressure at constant volume). Such approaches are required only when deficiencies in the density functional necessitate including this level of empiricism. In this work, we have demonstrated that accurate coordination numbers are predicted by the SCAN functional completely *ab initio*, without using any experimental information to inform the predictions, unlike what is necessary for LDA, for example.

Despite the differences in the average coordination numbers produced by the three functionals, fluctuations about that mean are insensitive to the choice of functional. Upon shifting the various $P(N_C)$ by the position of their respective means, the distributions collapse onto a single curve, as shown in the bottom panel of Fig. 3. This universal curve is well approximated by a Gaussian distribution near the mean [solid curve(s) in Fig. 3], but the distribution begins to deviate from Gaussianity far from the mean (if only slightly). The deviations of $P(N_C)$ from a Gaussian distribution can be understood by

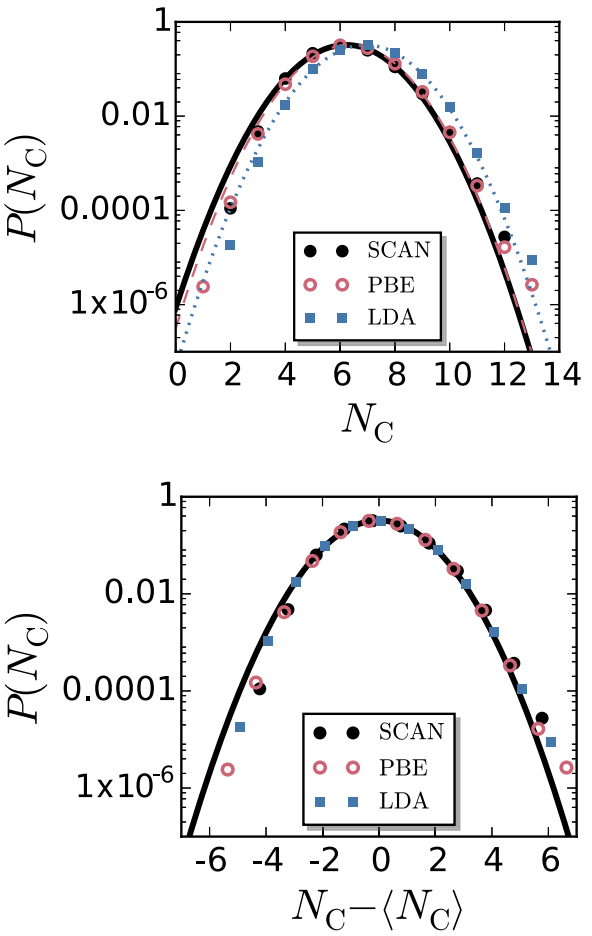

FIG. 3. (Top) Probability distribution $P(N_C)$ of the coordination number N_C around a silicon atom in the liquid. Lines are Gaussian distributions with the mean and variance determined from the simulations. (Bottom) $P(N_C)$ shifted by the respective means of the distribution, $\langle N_C \rangle$. Despite the differences in average coordination number among the functionals, all produce the same fluctuations in N_C. Moreover, deviations from Gaussian fluctuations begin to be observed at small and large N_C. A single Gaussian distribution is shown; all variances are similar.

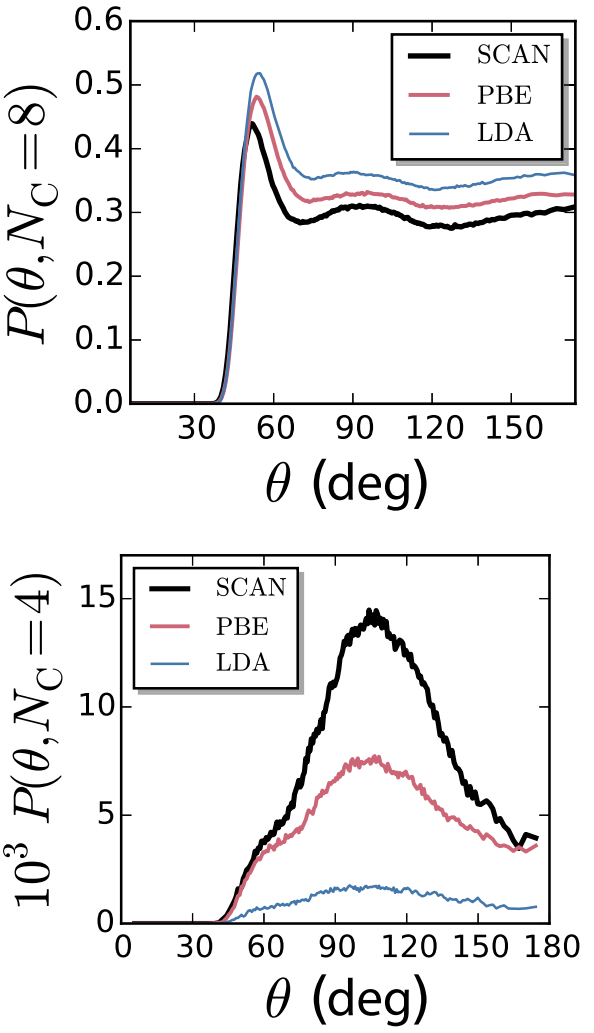

FIG. 4. Joint probability distributions of the angle θ and the number of nearest neighbors N_C for (top) $N_C = 8$ and (bottom) $N_C = 4$. The cutoff defining the nearest-neighbor shell is the distance of the first minimum in $g(r)$. Note that the variations in the solid angle ($\sin\theta$) have been removed.

considering how the nature of the interactions in the liquid change as a function of the coordination number.

Liquid Si exhibits both metallic and covalent bonding, the latter of which leads to tetrahedral coordination structures. A larger fraction of metallic bonding leads to disordered and higher coordination structures being more probable, consistent with the $P(N_C)$ produced by LDA, which predicts overly metallic systems. Examining the joint distribution $P(\theta, N_C)$ for fixed $N_C = 8$ or $N_C = 4$, Fig. 4, further supports this idea. $P(\theta, N_C)$ is the probability of simultaneously observing a triplet angle θ and a coordination number N_C for a given central atom, and it therefore describes the correlations between N_C and θ. We find that LDA has a larger population of disordered high-coordination structures than PBE and SCAN, with SCAN having the least. This trend is reversed for $N_C = 4$. Increasing the amount of covalent bonding, and consequently the fraction of tetrahedrally coordinated atoms, reduces N_C, as in SCAN and PBE. Indeed, the joint probability distribution $P(\theta, N_C = 4)$ indicates that SCAN has the highest population of four-coordinated tetrahedral structures, while LDA has the lowest with roughly an order of magnitude lower population (Fig. 4).

These ideas are also reflected in the deviations of $P(N_C)$ from a single Gaussian distribution, which averages over these metallic and covalent structures. To explain these deviations, we adopt the point of view that high coordination structures are correlated with metallic bonding and low N_C is due to covalent bonding, which is supported by the above results. From this perspective, the sub-Gaussian deviations at low N_C are a result of decreased fluctuations in covalently bonded tetrahedral environments. In contrast, enhanced fluctuations at high N_C arise from a higher population of atoms interacting through nondirectional metallic interactions, in comparison to the equilibrium populations of metallic and covalent species that lead to $\langle N_C \rangle$.

We conclude by noting that understanding such fluctuations are important for understanding chemical potentials and other solvationlike thermodynamic properties in atomic and

molecular systems [33–35] Determining such properties with high accuracy, however, requires advanced sampling techniques [36–38] and is beyond the scope of the current work.

B. Thermodynamics

We now focus on the accuracy with which each model of l-Si can reproduce the bulk density, ρ, computed from the average volume of the NPT-ensemble simulations, $\rho = N/\langle V\rangle$. This yields $\rho^{\mathrm{LDA}} = 2.70 \pm 0.07$ g/cm^{-3}, $\rho^{\mathrm{PBE}} = 2.54 \pm 0.08$ g/cm^{-3}, and $\rho^{\mathrm{SCAN}} = 2.57 \pm 0.08$ g/cm^{-3} for LDA, PBE, and SCAN, respectively, and the error bars indicate one standard deviation. The experimentally determined density typically cited [39] is $\rho = 2.56$ g/cm^{-3}, indicating that SCAN most accurately reproduces the experimental density of l-Si. However, we note that a wide range (2.2% deviation) of experimentally determined densities have been reported in the literature [40]. The PBE result falls into this range of experimental accuracy; the LDA predicted density is much too high.

The high density in the case of LDA is due to the inability of this approximation to properly describe covalent bonding. A non-neglible fraction of covalent interactions exists in the metallic liquid state of Si, which lead to tetrahedrally coordinated atoms and a more open liquid structure, thereby reducing the density. Both SCAN and PBE improve the description of such interactions. Thus we attribute the successful reproduction of the density by SCAN and PBE to a better description of the competition between covalent and metallic bonding in l-Si with respect to that provided by the LDA treatments.

The agreement between the experimental and SCAN densities may seem to be in contradiction to the differences between the pair correlation functions discussed above. This discrepancy can be resolved by examining the distance dependence of the coordination number, N_{C}, by varying the upper limit of integration in Eq. (2). For two systems with the same bulk density, equal values of N_{C} must be obtained as $g(r) \to 1$. Indeed, both SCAN and the experimental results yield the same value of N_{C} as $g(r)$ approaches unity, after integrating over the out of phase oscillations, and therefore the densities of the two systems are in agreement.

The use of the NPT ensemble enables the estimation of isothermal compressibilities from volume fluctuations,

$$\kappa_T = \beta \frac{\langle \delta V^2 \rangle}{\langle V \rangle}, \tag{3}$$

where κ_T is the isothermal compressibility, $1/\beta = k_{\mathrm{B}}T$, k_{B} is Boltzmann's constant, and $\delta V = V - \langle V\rangle$ is the deviation in the system volume from its average value. We find $\rho k_{\mathrm{B}} T \kappa_T^{\mathrm{SCAN}} \approx 0.047 \pm 0.008$, $\rho k_{\mathrm{B}} T \kappa_T^{\mathrm{PBE}} \approx 0.041 \pm 0.004$, and $\rho k_{\mathrm{B}} T \kappa_T^{\mathrm{LDA}} \approx 0.032 \pm 0.005$. The SCAN functional leads to the most compressible liquid, while the LDA l-Si is the least. This may simply be a consequence of LDA being more densely packed, while SCAN leads to a more open, low-density structure that can more readily be deformed. Similar arguments hold for the differences between LDA and PBE.

C. Atomic dynamics

The difference in interatomic interactions among the three density functional approximations will also impact the nature of the dynamics in l-Si. Here, we focus on the impact of density functional on self-diffusion in l-Si. We first examine the mean squared displacement (MSD),

$$\mathrm{MSD}(t) = \langle [\mathbf{r}(t) - \mathbf{r}(0)]^2 \rangle, \tag{4}$$

and this is compared in Fig. 5 for LDA, PBE, and SCAN. Diffusion coefficients, D, were obtained by fitting the long time behavior ($2 < t < 8$ ps) of MSD(t) to $6Dt + c$, and are listed in Table I. All descriptions of l-Si studied yield D values lower than that obtained from experiment [41], with SCAN being the lowest. This is not unexpected, since the SCAN description of l-Si is the most highly ordered and has the most covalent bonding between atoms. The increased population of tetrahedral, covalently bound neighbors, as quantified above, slows diffusion. LDA yields the fastest dynamics, consistent with that liquid having the least amount of covalent character. We note that we are aware of only a single D measurement for l-Si [41], and we encourage further measurements to confirm the experimental value of D.

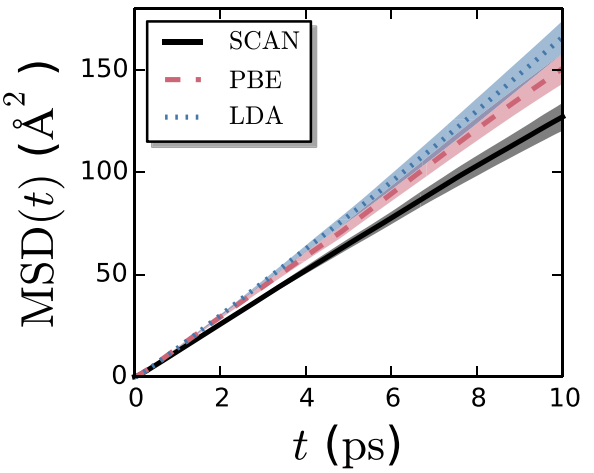

FIG. 5. Mean squared displacement, MSD(t), for SCAN, LDA, and PBE descriptions of l-Si. Shaded regions indicate one standard error obtained from block averaging.

Figure 6 shows the normalized velocity autocorrelation function,

$$C_v(t) = \frac{\langle \mathbf{v}(t) \cdot \mathbf{v}(0) \rangle}{\langle \mathbf{v}(0) \cdot \mathbf{v}(0) \rangle}, \tag{5}$$

as well as its power spectrum, $\tilde{C}_v(\omega)$, the phonon density of states. $C_v(t)$ obtained for each description of l-Si displays the same qualitative features, including a fast oscillatory

TABLE I. Diffusion coefficients (D) from the three exchange-correlation (XC) functionals studied and experiments. Uncertainty in computed values corresponds to one standard error obtained from block averaging.

XC	D (Å^2/ps)
SCAN	2.2 ± 0.4
PBE	2.6 ± 0.5
LDA	2.8 ± 0.7
Expt. [41]	4 ± 0.5

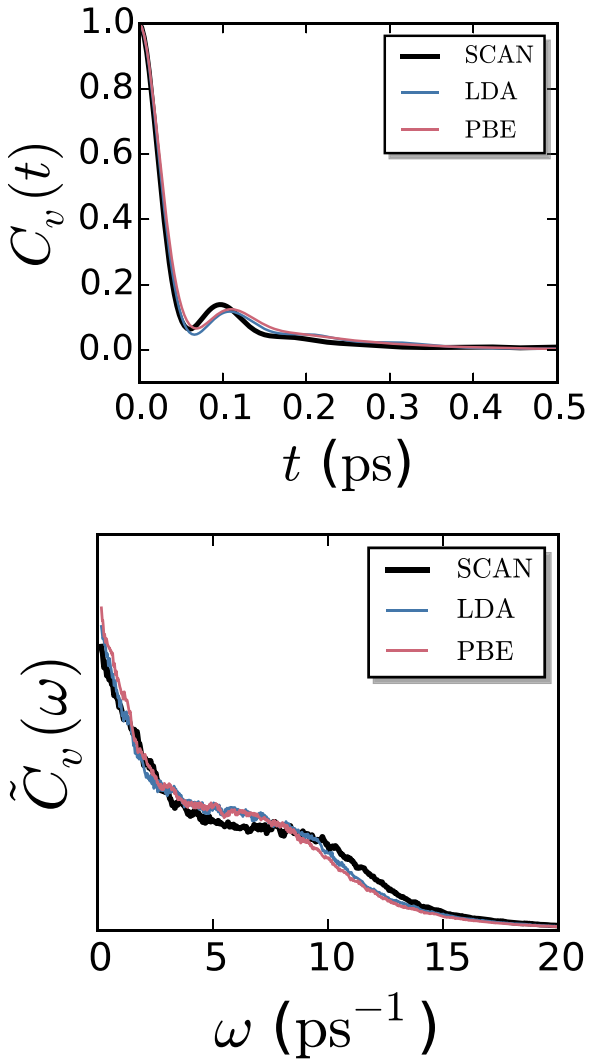

FIG. 6. (Top) Velocity autocorrelation functions, $C_v(t)$, and (bottom) the corresponding power spectra, $\tilde{C}(\omega)$, for SCAN, LDA, and PBE descriptions of l-Si.

decay that remains positive. This has been attributed to the open structure of l-Si, which contrasts the close-packed-like structure of simple liquids that leads to negative oscillations in $C_v(t)$ [1,10,42]. The more pronounced oscillation in the $C_v(t)$ obtained from SCAN, with respect to LDA and PBE, can thus be explained by the increase in covalent bonding with its neighbors, leading to a more open coordination structure.

The power spectra (phonon density of states) shown in Fig. 6(b) also exhibit the same qualitative features across functionals. Namely, low-frequency diffusive modes and higher-frequency vibrational modes reflecting covalent bonding are found in all $\tilde{C}_v(\omega)$. However, the higher-frequency modes are more pronounced in the SCAN l-Si, in accord with the increased covalency of this system.

D. Collective dynamics

We quantify the collective dynamics in l-Si through the intermediate scattering function

$$F_k(t) = \langle \rho_{\mathbf{k}}(t)\rho_{-\mathbf{k}}(0)\rangle, \tag{6}$$

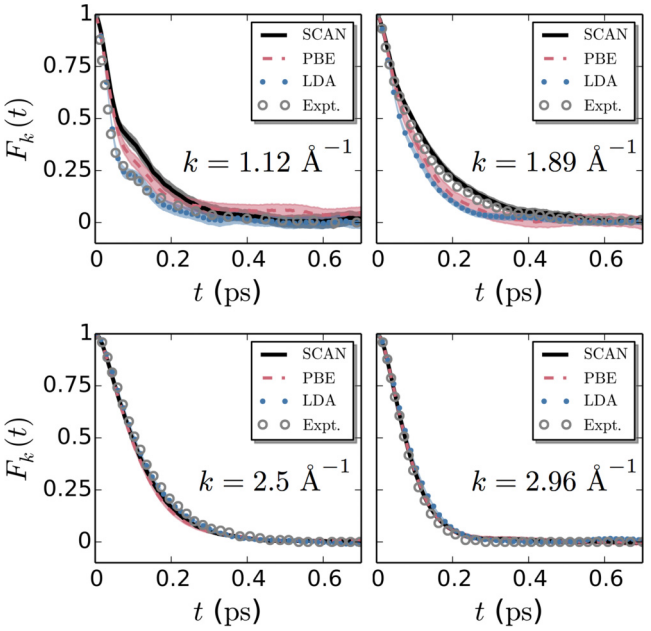

FIG. 7. Intermediate scattering functions, $F_k(t)$, for LDA, PBE, and SCAN descriptions of l-Si at wave vectors $k =$ 1.12, 1.89, 2.5, and 2.96 Å^{-1}. Also shown are results from inelastic x-ray scattering measurements [43,44]. Shaded regions correspond to one standard deviation.

where

$$\rho_{\mathbf{k}}(t) = \frac{1}{\sqrt{N}} \sum_{j=1}^{N} e^{i\mathbf{k}\cdot\mathbf{r}_j(t)} \tag{7}$$

is a Fourier component of the density. We compare the predictions obtained for $F_k(t)$ with the inelastic x-ray scattering measurements of Hosokawa *et al.* [43,44]. Due to the finite system sizes employed in the simulations, we are limited to $k \geqslant 2\pi/L$, where L is the average length of the fluctuating cubic simulation cell, and we cannot reach the lowest k values probed experimentally. That is, we are prohibited from studying the purely hydrodynamic, low k regime of $F_k(t)$ with good accuracy. Moreover, because the simulation cell is fluctuating, we average over allowable k values within a range of 0.1 Å^{-1}. The computed intermediate scattering functions do not change appreciably within this range of k.

The intermediate scattering functions for LDA, PBE, and SCAN descriptions of l-Si are compared in Fig. 7 for $k =$ 1.12, 1.89, 2.5, and 2.96 Å^{-1}. At the lowest k value probed, LDA agrees well with the x-ray measurements, while the decay of $F_k(t)$ produced by SCAN is too slow; PBE falls between SCAN and LDA. This value of k corresponds approximately to the third peak of $g(r)$. Thus $F_k(t)$ probes dynamic correlations between particles separated by a coordination shell. These correlations are predominantly between noncovalently bonded atoms. Within the SCAN description of l-Si, such interactions are weighted less than expected from experiments, slowing the time decay of correlations. In contrast, LDA accurately describes such correlations, and agrees with the experiments.

As the first peak in $S(k)$ is approached, $k = 1.89$ Å^{-1}, the situation is reversed. The intermediate scattering function

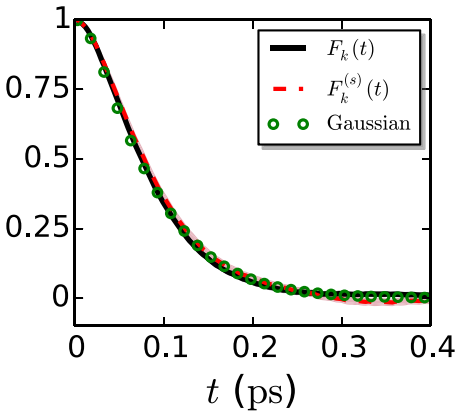

FIG. 8. Intermediate scattering functions, $F_k(t)$, self-intermediate scattering function, $F_k^{(s)}(t)$, and the Gaussian approximation to the self-part from Eq. (9) for the SCAN description of l-Si at $k = 2.96$ Å^{-1}. Shaded regions correspond to one standard deviation.

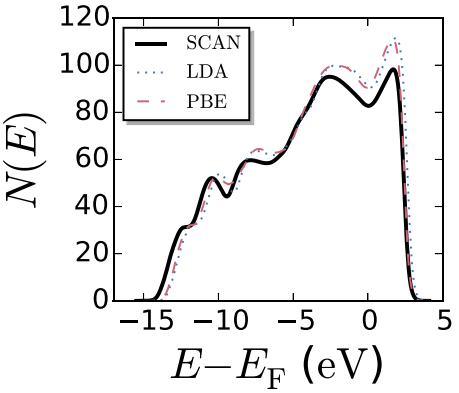

FIG. 9. Densities of states $N(E)$ averaged over trajectories for SCAN, PBE, and LDA descriptions of l-Si. All $N(E)$ are shifted by their respective Fermi energies.

produced by LDA decays quicker than the experimental data, while the SCAN $F_k(t)$ is in agreement with the experimental results. This value of k is within the length scales indicative of correlations between covalently bonded atoms, roughly $1.4 \leqslant k \leqslant 1.9$ Å^{-1}. Thus $F_k(t)$ on this length scale is probing the space-time correlations between covalently bonded atoms in the liquid. The SCAN meta-GGA improves the descriptions of these atoms and their spatial correlations beyond that provided by LDA and PBE, and one would expect that this improvement also yields a better description of the dynamic correlations as well, as evidenced here.

Near the peak in $S(k)$, $k = 2.5, 2.96$ Å^{-1}, $F_k(t)$ produced by all three functionals are in agreement with each other and the experimental data. On these scales, we find that $F_k(t) \approx F_k^{(s)}(t)$, where

$$F_k^{(s)}(t) = \frac{1}{N}\left\langle \sum_{j=1}^{N} e^{i\mathbf{k}\cdot[\mathbf{r}_j(t)-\mathbf{r}_j(0)]} \right\rangle \tag{8}$$

is the self-part of the intermediate scattering function. The self-intermediate scattering function describes single-particle dynamics, and so we might expect these functions to be quite similar for all three functionals based on the results in the previous section. Indeed, the self-intermediate scattering function can be well approximated by the Gaussian approximation involving the mean-squared displacement [42,45],

$$F_k^{(s)}(t) \approx \exp\left[-\frac{k^2 \mathrm{MSD(t)}}{6}\right], \tag{9}$$

as shown in Fig. 8. Because the experimentally determined $F_k(t)$ for these k values are in agreement with the simulation predictions, even at the level of the above Gaussian approximation involving the MSD, we may expect the diffusion coefficient of liquid Si to be closer to that predicted by simulation, and by SCAN in particular.

E. Electronic properties

In Fig. 9 we report the electronic density of states $N(E)$ averaged over the trajectories. All functionals yield metallic liquids, as evidenced by the absence of a gap in $N(E)$ at the Fermi level E_F. Moreover, the three functionals studied provide a quantitatively similar description of $N(E)$ when shifted by E_F. The low energy portions of $N(E)$ are similar for all functionals. Differences among the three functionals appear near the Fermi level. In the vicinity of E_F, $N(E)$ for SCAN is significantly lower than that for PBE and LDA, indicating that the SCAN description of l-Si is less metallic. This is consistent with SCAN producing more covalent character in the liquid.

IV. CONCLUSIONS

In this work, we have presented a thorough investigation of liquid silicon using *ab initio* molecular dynamics simulations. We have demonstrated that the discrimination between covalent and metallic bonding provided by the nonempirical SCAN meta-GGA leads to a good description of this complex liquid. Moreover, SCAN gives significant improvements over the conventional LDA and PBE functionals for the structural, thermodynamic, and electronic properties, although noticeable differences still exist between simulation and experiment which might arise from self-interaction errors present in SCAN. Such errors can lead to overbinding and, consequently, the discrepancies between the simulated and experimental $S(k)$, for example.

Removing self-interaction errors in the SCAN functional is an active area of research, but existing hybrid versions of SCAN have provided exceptional results by reducing such errors [46]. Despite these possible errors, we additionally find the dynamic predictions of SCAN of particular interest. SCAN predicts slower diffusion than both LDA and PBE, reducing D to a factor of two less than the single experimental result of which we are aware, while improving nearly every other aspect of l-Si. This counterintuitive results suggests that additional experiments to confirm the experimental value of the diffusion coefficient for l-Si are needed. Indeed, agreement between experimental intermediate scattering functions and those predicted by SCAN on intermediate wavelengths suggest that the dynamics produced by SCAN should be in closer agreement with experiments. Finally, we note that vdW interactions may also be important, especially to provide the cohesive energy that results in appropriate values of the bulk density [47,48]

(after self-interaction errors are remedied). Newly developed vdW corrections to SCAN hold great promise in this area [23,24].

ACKNOWLEDGMENTS

This work was supported as part of the Center for the Computational Design of Functional Layered Materials, an Energy Frontier Research Center funded by the US Department of Energy, Office of Science, Basic Energy Sciences under Grant No. DE-SC0012575. This research used resources of the National Energy Research Scientific Computing Center (NERSC), a DOE Office of Science User Facility supported by the Office of Science of the US Department of Energy. Additional computational resources were provided in part by the National Science Foundation through major research instrumentation Grant No. CNS-09-58854.

APPENDIX A: FINITE-SIZE EFFECTS

Because l-Si is metallic, significant finite-size effects may be expected. Thus we examine these effects using the SCAN functional by simulating systems with 64, 216 (the systems in the main text), and 512 atoms. Note that we only change the number of atoms, N, and not any other simulation parameters, including energy cutoffs and the number of k points.

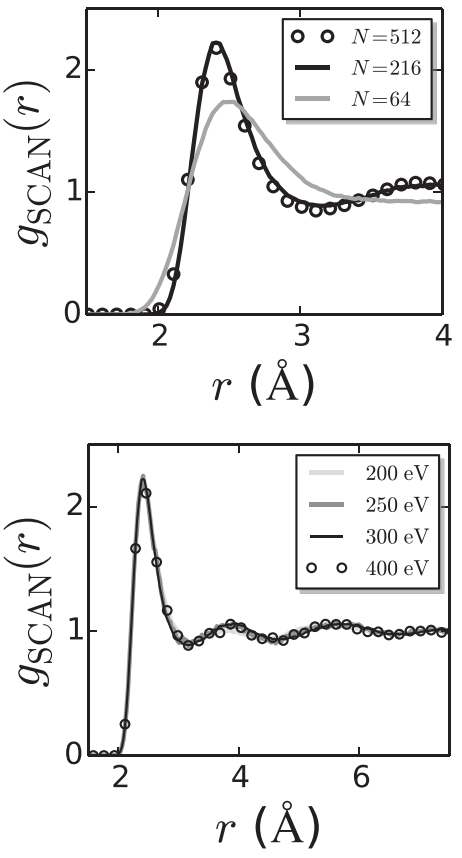

FIG. 10. (Top) Pair correlation functions, $g(r)$, for the SCAN description of l-Si for varying number of particles, N. (Bottom) Representative pair correlation functions, $g(r)$, for the SCAN density functional approximation for several values of the energy cutoff E_{cut}.

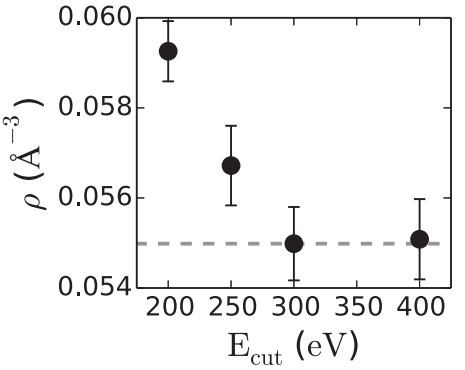

FIG. 11. Bulk density as a function of the plane wave cutoff E_{cut}. The dashed line indicates the value of the density reported in the main text and error bars indicate one standard deviation.

In all quantities studied here, significant differences are observed between the $N = 64$ system and the other two, suggesting that this system is too small (with the simulation parameters used). In contrast, the structure in the $N = 216$ and $N = 512$ systems are nearly identical, suggesting that finite size effects play a minimal role and $N = 216$ is large enough to make quantitative predictions. This is illustrated by the pair correlation functions, $g(r)$, shown in Fig. 10 as a representative example of convergence with respect to system size. The dynamic properties follow a similar trend, and are converged at $N = 216$.

APPENDIX B: CONVERGENCE STUDY

In this appendix, we present the results of our study to monitor convergence of the systems with respect to the simulation parameters employed, namely the energy cutoff and the number of k points. This was performed by monitoring the structural properties of the systems (all functionals) when varying the energy cutoff E_{cut}; we set $E_{\mathrm{cut}} = 200$, 250, 300, and 400 eV. We also explored changing the Brillouin zone sampling from Γ point only, $\mathbf{k} = (0,0,0)$, to a $4 \times 4 \times 4$ k-point mesh.

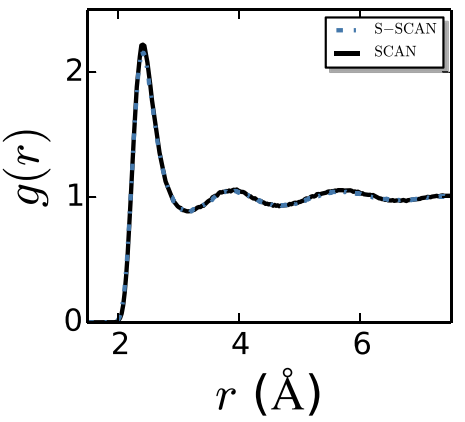

FIG. 12. Pair distribution function $g(r)$ for the SCAN description of l-Si and that including spin polarization (S-SCAN). The two curves lie on top of one another.

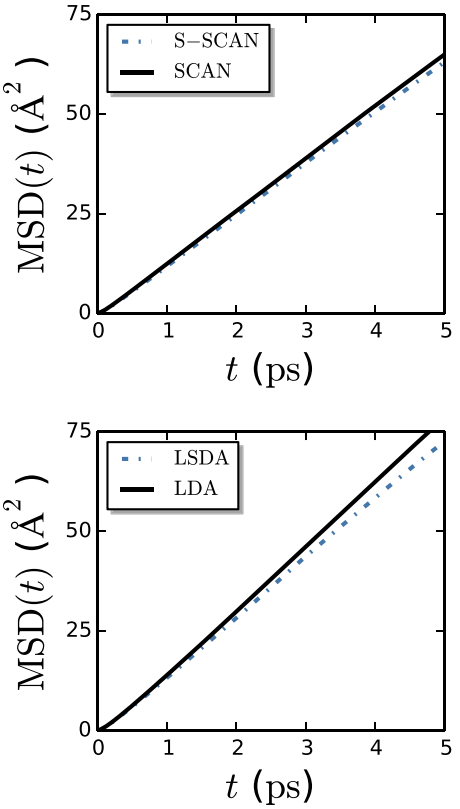

FIG. 13. Mean squared displacements of l-Si using (top) the SCAN functional and (bottom) LDA, both with and without spin polarization.

Pair correlation functions for various values of E_{cut} are shown in Fig. 10 for the SCAN functional. We find that the SCAN functional converges near $E_{\text{cut}} = 300$ eV, while LDA and PBE converge at lower values; we simulated all functionals with $E_{\text{cut}} = 300$ eV in the results presented in the main text for consistency. Additionally, changing the Brillouin zone sampling from the Γ point only to a larger k-point mesh had little impact on the properties of the systems at a fixed value of E_{cut}.

We also examined how properties such as the bulk density ρ depend on E_{cut}, as shown in Fig. 11. The pressure, and therefore the density, is quite sensitive to the value of E_{cut}, such that convergence typically requires larger values of a cutoff to converge than other properties. We find that the density is converged at $E_{\text{cut}} = 300$ eV, and that this quantity does not change upon increasing the cutoff to 400 eV. We also note that $g(r)$ is essentially converged at $E_{\text{cut}} = 250$ eV, despite the system having too large a density, illustrating that the density (or equivalently the pressure) requires larger cutoffs to converge than other properties as found in previous work [17].

APPENDIX C: EFFECTS OF SPIN POLARIZATION

Previous work has concluded that including the effects of spin polarization can impact the predicted properties of l-Si [10]. Therefore, we additionally probed the impact of including a description of spin-polarization by running simulations with spin-polarized variants of SCAN (S-SCAN) and LDA (LSDA). The S-SCAN trajectory examined is 23.9 ps in duration, while that for LSDA is 15 ps.

As indicated by the S-SCAN and SCAN pair distribution functions in Fig. 12, we find that the structure of the system is insensitive to spin polarization; analogous results were found for LSDA and LDA. As discussed previously [10], the average spin is zero and spin fluctuations are significant mainly during bond breakage and reformation. These large temporal fluctuations in the spin average to zero, and one might expect that their impact on the average structure should then be small. Indeed, this is what we observe. However, such fluctuations should impact dynamics significantly. We find that spin fluctuations slow the dynamics of both SCAN and LDA descriptions of l-Si by strengthening bonding in liquid silicon, evidenced by the MSDs shown in Fig. 13. This is in accord with the earlier interpretation [10] that spin polarization adds additional attractions. We also note that this increases the discrepancy between the single experimental measurement of the diffusion coefficient quoted here [41] and the computed values, furthering the need for additional experimental studies of the dynamics of l-Si.

[1] I. Štich, R. Car, and M. Parrinello, Phys. Rev. B **44**, 4262 (1991).
[2] W. Jank and J. Hafner, Phys. Rev. B **41**, 1497 (1990).
[3] J. T. Okada, P. H.-L. Sit, Y. Watanabe, Y. J. Wang, B. Barbiellini, T. Ishikawa, M. Itou, Y. Sakurai, A. Bansil, R. Ishikawa, M. Hamaishi, T. Masaki, P.-F. Paradis, K. Kimura, T. Ishikawa, and S. Nanao, Phys. Rev. Lett. **108**, 067402 (2012).
[4] S. S. Ashwin, U. V. Waghmare, and S. Sastry, Phys. Rev. Lett. **92**, 175701 (2004).
[5] P. Ganesh and M. Widom, Phys. Rev. Lett. **102**, 075701 (2009).
[6] S. Sastry and C. Austen Angell, Nat. Mater. **2**, 739 (2003).
[7] V. V. Vasisht, S. Saw, and S. Sastry, Nat. Phys. **7**, 549 (2011).
[8] S. Sastry, Proc. Natl. Acad. Sci. USA **107**, 17063 (2010).
[9] D. Alfè and M. J. Gillan, Phys. Rev. B **68**, 205212 (2003).
[10] I. Štich, M. Parrinello, and J. M. Holender, Phys. Rev. Lett. **76**, 2077 (1996).
[11] I. Štich, R. Car, and M. Parrinello, Phys. Rev. Lett. **63**, 2240 (1989).
[12] O. Sugino and R. Car, Phys. Rev. Lett. **74**, 1823 (1995).
[13] P. F. McMillan, M. Wilson, D. Daisenberger, and D. Machon, Nat. Mater. **4**, 680 (2005).
[14] N. Jakse and A. Pasturel, J. Chem. Phys. **129**, 104503 (2008).
[15] T. Morishita, Phys. Rev. E **72**, 021201 (2005).
[16] T. Morishita, Phys. Rev. Lett. **93**, 055503 (2004).
[17] T. Morishita, Phys. Rev. Lett. **97**, 165502 (2006).
[18] J. P. Perdew, K. Burke, and M. Ernzerhof, Phys. Rev. Lett. **77**, 3865 (1996).
[19] J. Sun, B. Xiao, Y. Fang, R. Haunschild, P. Hao, A. Ruzsinszky, G. I. Csonka, G. E. Scuseria, and J. P. Perdew, Phys. Rev. Lett. **111**, 106401 (2013).

[20] J. Sun, R. C. Remsing, Y. Zhang, Z. Sun, A. Ruzsinszky, H. Peng, Z. Yang, A. Paul, U. Waghmare, X. Wu, M. L. Klein, and J. P. Perdew, Nat. Chem. **8**, 831 (2016).
[21] J. Sun, A. Ruzsinszky, and J. P. Perdew, Phys. Rev. Lett. **115**, 036402 (2015).
[22] D. A. Kitchaev, H. Peng, Y. Liu, J. Sun, J. P. Perdew, and G. Ceder, Phys. Rev. B **93**, 045132 (2016).
[23] H. Peng, Z.-H. Yang, J. P. Perdew, and J. Sun, Phys. Rev. X **6**, 041005 (2016).
[24] J. G. Brandenburg, J. E. Bates, J. Sun, and J. P. Perdew, Phys. Rev. B **94**, 115144 (2016).
[25] G. Kresse and J. Furthmüller, Phys. Rev. B **54**, 11169 (1996).
[26] P. E. Blöchl, Phys. Rev. B **50**, 17953 (1994).
[27] P. J. Steinhardt, D. R. Nelson, and M. Ronchetti, Phys. Rev. B **28**, 784 (1983).
[28] M. Parrinello and A. Rahman, J. Appl. Phys. **52**, 7182 (1981).
[29] P. Langevin, C. R. Acad. Sci. Paris **146**, 530 (1908).
[30] D. S. Lemons and A. Gythiel, Am. J. Phys. **65**, 1079 (1997).
[31] Y. Waseda, K. Shinoda, K. Sugiyama, S. Takeda, K. Terashima, and J. M. Toguri, Jpn. J. Appl. Phys. **34**, 4124 (1995).
[32] R. C. Remsing, M. L. Klein, and J. Sun (unpublished).
[33] B. Widom, J. Phys. Chem. **86**, 869 (1982).
[34] B. Widom, J. Chem. Phys. **39**, 2808 (1963).
[35] T. L. Beck, M. E. Paulaitis, and L. R. Pratt, *The Potential Distirbution Theorem and Models of Molecular Solutions* (Cambridge University Press, Cambridge, UK, 2006).
[36] A. J. Patel and S. Garde, J. Phys. Chem. B **118**, 1564 (2014).
[37] A. J. Patel, P. Varilly, D. Chandler, and S. Garde, J. Stat. Phys. **145**, 265 (2011).
[38] E. Xi, R. C. Remsing, and A. J. Patel, J. Chem. Theory Comput. **12**, 706 (2016).
[39] H. Sasaki, E. Tokizaki, K. Terashima, and S. Kimura, Jpn. J. Appl. Phys. **33**, 3803 (1994).
[40] M. J. Assael, I. J. Armyra, J. Brillo, S. V. Stankus, J. Wu, and W. A. Wakeham, J. Phys. Chem. Ref. Data **41**, 033101 (2012).
[41] P. G. Sanders and M. J. Aziz, J. Appl. Phys. **86**, 4258 (1999).
[42] J. P. Hansen and I. R. McDonald, *Theory of Simple Liquids* (Elsevier Ltd., Amsterdam, 2006).
[43] S. Hosokawa, W.-C. Pilgrim, Y. Kawakita, K. Ohshima, S. Takeda, D. Ishikawa, S. Tsutsui, Y. Tanaka, and A. Q. R. Baron, J. Phys.: Condens. Matter **15**, L623 (2003).
[44] S. Hosokawa, W.-C. Pilgrim, Y. Kawakita, S. Takeda, A. Q. R. Baron, D. Ishikawa, and S. Tsutsui, J. Non-Cryst. Solids **353**, 3149 (2007).
[45] T. Morishita, J. Chem. Phys. **137**, 024510 (2012).
[46] K. Hui and J.-D. Chai, J. Chem. Phys. **144**, 044114 (2016).
[47] R. C. Remsing, J. M. Rodgers, and J. D. Weeks, J. Stat. Phys. **145**, 313 (2011).
[48] R. C. Remsing and J. D. Weeks, J. Phys. Chem. B **117**, 15479 (2013).